A Study of the Characteristics and Assimilation of Retrieved MODIS Total Precipitable Water Data in Severe Weather Simulations

SHU-HUA CHEN

Department of Land, Air, and Water Resources, University of California, Davis, Davis, California, and Department of Atmospheric Sciences, National Central University, Chung-Li, Taiwan

ZHAN ZHAO

Department of Land, Air, and Water Resources, University of California, Davis, Davis, California

JENNIFER S. HAASE

Department of Earth and Atmospheric Sciences, Purdue University, West Lafayette, Indiana

AIDONG CHEN

Department of Land, Air, and Water Resources, University of California, Davis, Davis, California

FRANCOIS VANDENBERGHE

National Center for Atmospheric Research, Boulder, Colorado

(Manuscript received 21 September 2007, in final form 16 January 2008)

ABSTRACT

This study determined the accuracy and biases associated with retrieved Moderate Resolution Imaging Spectroradiometer (MODIS) total precipitable water (TPW) data, and it investigated the impact of these data on severe weather simulations using the Weather Research and Forecast (WRF) model. Comparisons of MODIS TPW with the global positioning system (GPS) TPW and radiosonde-derived TPW were carried out. The comparison with GPS TPW over the United States showed that the root-mean-square (RMS) differences between these two datasets were about 5.2 and 3.3 mm for infrared (IR) and near-infrared (nIR) TPW, respectively. MODIS IR TPW data were overestimated in a dry atmosphere but underestimated in a moist atmosphere, whereas the nIR values were slightly underestimated in a dry atmosphere but overestimated in a moist atmosphere.

Two cases, a severe thunderstorm system (2004) over land and Hurricane Isidore (2002) over ocean, as well as conventional observations and Special Sensor Microwave Imager (SSM/I) retrievals were used to assess the impact of MODIS nIR TPW data on severe weather simulations. The assimilation of MODIS data has a slightly positive impact on the simulated rainfall over Oklahoma for the thunderstorm case, and it was able to enhance Isidore's intensity when the storm track was reasonably simulated. The use of original and bias-corrected MODIS nIR TPW did not show significant differences from both case studies. In addition, SSM/I data were found to have a positive impact on both severe weather simulations, and the impact was comparable to or slightly better than that of MODIS data.

1. Introduction

In the past two decades, remote sensing instruments (e.g., radar and satellites) have added a tremendous amount of data to existing observation networks. This is leading to important advances in our knowledge of the dynamics and physics of weather phenomena (Huang et al. 2006; Wang and Michelangeli 2006), improvements in weather simulations and forecasts (i.e., Gerard and Saunders 1999; Hou et al. 2000; Pu and Braun 2001; Leidner et al. 2003; Chen et al. 2004; Isaksen and Janssen 2004; Huang et al. 2005; Zhang et al. 2007), and support for the study of climate change (Lau and Chan 1983; Andrew 1987; Steffen et al. 1993; Chelton and Wentz 2005). Improvements in the ability to

Corresponding author address: Shu-Hua Chen, Department of Land, Air, and Water Resources, University of California, Davis, Davis, CA 95616-8627.
E-mail: shachen@ucdavis.edu

DOI: 10.1175/2008MWR2384.1

observe the distribution and propagation of atmospheric moisture play a critical role in these advances. Many instruments on board satellites have been monitoring atmospheric moisture information, such as the Special Sensor Microwave Imager (SSM/I), the Geostationary Operational Environmental Satellite (GOES), the Microwave Sounding Unit (MSU), the Humidity Sounder for Brazil (HSB), the Atmospheric Infrared Sounder (AIRS), and the Moderate Resolution Imaging Spectroradiometer (MODIS). Instruments that detect infrared (IR) frequencies (e.g., GOES and AIRS) can measure moisture over land and ocean in cloud-free regions. Instruments that use microwave frequencies (e.g., SSM/I, HSB, and MSU) can measure moisture under both clear and cloudy conditions but only over ocean. These microwave data, however, can be contaminated by heavy precipitation. MODIS is the first space instrument that uses near-infrared (nIR) bands, together with the traditional IR bands, to obtain total precipitable water (TPW) data over land and ocean in cloud-free regions and above cloud tops in cloudy regions (the latter only for nIR data). This study addresses the capabilities of the MODIS instruments in collecting moisture measurements and demonstrates their potential for contributing to improvements in weather simulations, in particular data retrieved from nIR channels.

Both the *Terra* satellite (launched December 1999) and the *Aqua* satellite (launched May 2002) are equipped with the MODIS scanning spectroradiometer. MODIS detects electromagnetic radiation in 36 spectral bands between 0.4 and 14.4 μm with spatial resolutions of 250 (2 bands), 500 (5 bands), and 1000 m (29 bands; King et al. 1992). The swath width of the MODIS data is 2300 for *Terra* and 2330 km for *Aqua*, and the satellites are in polar sun-synchronous orbit at an altitude of 705 km. The retrieved nIR MODIS TPW, which is available during daytime only, is derived from two water vapor absorption bands centered near 0.905 and 0.94 μm and three water vapor window bands centered near 0.865, 0.936, and 1.24 μm. The ratio of reflected solar radiances from an absorption channel and a window channel is used to derive atmospheric water vapor transmittances; the column TPW is then obtained from the transmittances using a lookup table that was precalculated with a line-by-line atmospheric transmittance code (Kaufman and Gao 1992; King et al. 2003). The quality of MODIS nIR TPW relies on observed water vapor attenuation of nIR solar radiation, which is reflected by surfaces and clouds. Therefore, the accuracy of retrieved MODIS nIR TPW data strongly depends on the estimation of surface reflection. A larger error can be introduced over regions where surface reflection is small in nIR channels, such as the ocean, except for sun-glint areas where the surface reflectance is relatively high (Kleidman et al. 2000).

The retrieved MODIS IR TPW is derived from bands 24 to 36 (between 4.47 and 14.24 μm), excluding band 26, and it is available during both the day and night. A statistical regression algorithm, with an option of a subsequent nonlinear physical retrieval, is used to retrieve atmospheric temperature, moisture, ozone profiles, and skin temperature (Seemann et al. 2003). Through the use of a linearized radiative transfer model and the inversion of radiance measurements, the regression coefficients were derived from a set of global radiosonde soundings and the radiances that were computed from those soundings. The linearized radiative transfer model has 101 pressure levels from 0.05 to 1100 hPa. Therefore, retrieved vertical moisture profiles have the same number of levels, which are then used to integrate the MODIS IR TPW.

Several studies of MODIS TPW data have contributed to satellite commission and calibration. Kaufman and Gao (1992) showed that the error of the airborne version of MODIS nIR TPW was as low as 7% after the incorporation of additional MODIS channels that reduced the effects of uncertainties in surface reflectance, subpixel clouds, haze, and temperature profile on the derived water vapor. Based on theoretical calculations and lookup tables, Gao and Kaufman (2003) estimated that the error of MODIS nIR TPW was about 5%–10%. Kleidman et al. (2000) compared MODIS nIR TPW from the MODIS Airborne Simulator with that from the differential infrared absorption lidar system on board the National Aeronautics and Space Administration (NASA) ER-2 research aircraft over ocean sun-glint regions. They found that the error of estimated MODIS nIR TPW was about 5 mm, and the TPW amounts were underestimated when the column water vapor content was relatively low. Seemann et al. (2003) compared the MODIS IR TPW data from *Aqua* and *Terra* with that from SSM/I, GOES, radiosondes, and the ground-based microwave radiometer (MWR) at the Atmospheric Radiation Measurement (ARM) Program Cloud and Radiation Test Bed (CART) in Oklahoma. Their results from the comparison with MWR data showed that the root-mean-square (RMS) error of the regression-based MODIS IR TPW was 4.1 mm. For a dry atmosphere, retrieved MODIS IR TPW, using either physical or regression-based algorithms, was overestimated by 3.7 mm on average, and for a moist atmosphere it was underestimated by 1.2 mm.

With these high spatial resolution data, it was hoped that MODIS TPW would be able to improve weather forecasts. However, relatively few studies beyond

MODIS TPW data comparison and calibration have been carried out so far. Zhang et al. (2007) assimilated retrieved temperature and dewpoint soundings from MODIS IR channels for Hurricane Lili (2002) simulations, and the simulated storm intensity was slightly improved. Although the assimilation of satellite data is challenging, many studies with other instruments have shown improvements of weather simulations–forecasts (Gerard and Saunders 1999; Deblonde 1999; Xiao et al. 2000; Chen et al. 2004; Lagouvardos and Kotroni 2005; Zhang et al. 2007; Chen 2007), whereas a smaller number of cases showed a negative impact or almost no improvement (Zou et al. 2001). The assimilation of MODIS TPW is expected to be equally or more challenging because of the potential for data biases and the difficulty of cloud mask determination.

This work deals with developing and testing of the assimilation of MODIS nIR TPW and some of the challenges associated with this particular dataset. The error characteristics of MODIS nIR and IR TPW are analyzed by comparing them with independent observations from the ground-based global positioning system (GPS) in the United States and from computed TPW from radiosonde soundings in the United States and Australia in section 2. The Weather Research and Forecasting (WRF) model variational data assimilation (VAR) system (Skamarock et al. 2005) used for the testing, its configuration, and the experimental design are introduced in section 3. Some preliminary results assessing the impact of assimilating MODIS nIR TPW using two severe weather cases are in section 4, and some brief concluding remarks are in section 5.

2. Observations and data comparison

a. Data

An example of the MODIS level-2 nIR and IR TPW data (MOD05 products; Gao and Kaufman 2003; Seemann et al. 2003) from the *Aqua* satellite granule between 1840 and 1845 UTC 19 September 2002 at the time when Hurricane Isidore moved to the southwest of Cuba are shown in Fig. 1 (see white cross in Fig. 1b). MODIS IR data were void in cloudy regions, such as directly over Hurricane Isidore and its vicinity. MODIS nIR data were available in those regions, but the values were integrated only above the cloud top. Thus, they were significantly lower compared to the integration of the whole column. Therefore, the detection of cloudy pixels, and data quality control, can be crucial when assimilating MODIS nIR TPW data.

The MODIS TPW data have a spatial resolution of 1 and 5 km for nIR and IR TPW, respectively. To make both datasets comparable, MODIS nIR data were

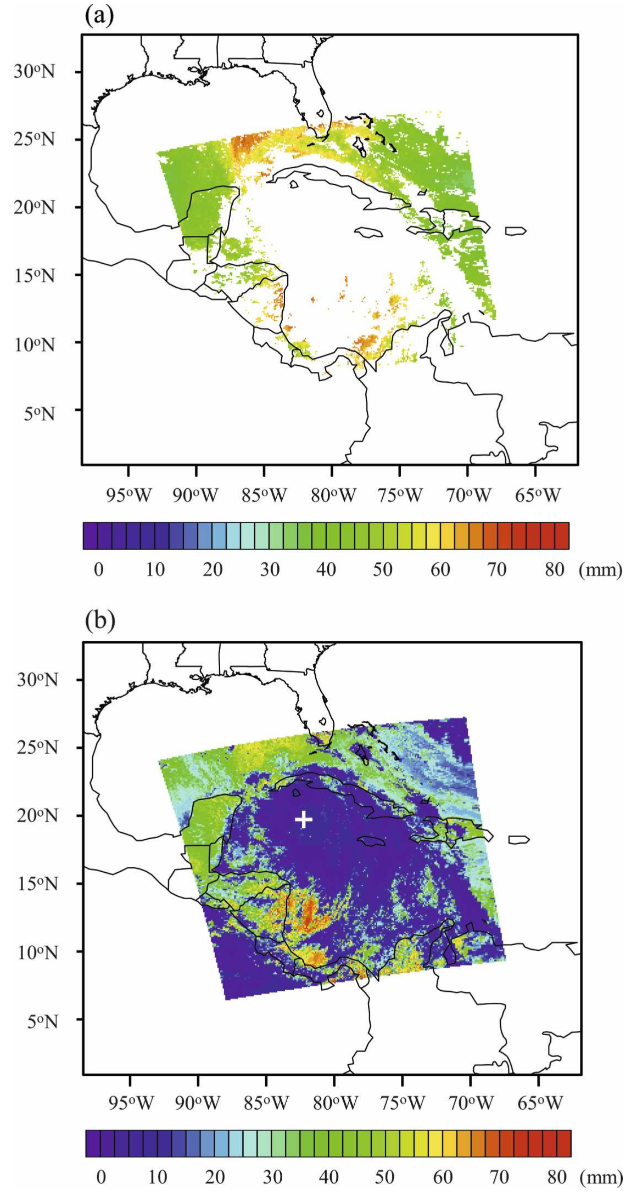

FIG. 1. MODIS (a) IR and (b) nIR TPW (mm) for the granule from 1840 to 1845 UTC 19 Sep 2002. The white cross is the central location of Hurricane Isidore at this time.

smoothed to a 5-km resolution by averaging data from cloud-free pixels in 5 × 5 matrices, with a required minimum of 10 clear-sky pixels identified using the cloudiness flag provided in the dataset. To understand the characteristics of the retrieved MODIS TPW and to better use those data in assimilation, the IR and nIR data were compared with two independent observations over different regions: retrieved TPW from ground-based GPS receivers and computed TPW from radiosondes.

GPS TPW is the primary reference dataset for the comparisons because it is available continuously at 15-min sampling during all weather conditions, so it is always available for comparison for every satellite pass, whereas radiosonde comparisons are usually only possible at 0000 and 1200 UTC. When the GPS TPW technique was developed, the first comparison with microwave radiometers by Rocken et al. (1993) demonstrated accuracy at the level of 1 kg m^{-2}. Since then, many validation studies have been carried out with GPS data against other datasets, such as microwave radiometers and radiosondes (see Haase et al. 2003 and their references). In that study, data from 58 sites in Europe were used to demonstrate consistency among different processing algorithms of 6 mm in zenith tropospheric delay (equivalent to ~1 mm TPW) and a standard deviation of 12 mm in zenith tropospheric delay (equivalent to ~2 mm TPW) when compared to radiosonde data. In addition, this study showed that the GPS TPW data were not sensitive to daytime biases in TPW due to radiation heating as radiosondes were. Comparable studies were carried out for sites in the continental United States that were used in the present study (Smith et al. 2000). Further studies comparing GPS data and radiosondes (Liljegren et al. 1999) contributed to the discovery and characterization of the dry bias of radiosondes (Wang et al. 2002). The practical convenience of the GPS TPW data and its demonstrated accuracy make it ideal for use as a reference dataset.

For GPS, data from 16 May to 9 June 2004 from 101 sites over the continental United States were retrieved from the National Oceanic and Atmospheric Administration (NOAA) Forecast System Laboratory (Gutman et al. 2004). For the radiosonde comparisons, soundings over the United States around 0600 and 1800 UTC from 2002 to 2005 were used. In addition, radiosondes from Australian stations (Fig. 2) were chosen because the satellites pass the eastern region of the country at the time when radiosondes were launched (around 0000 and 1200 UTC). Two months, January and July (summer and winter, respectively, in the Southern Hemisphere) 2003, were selected for the comparison. MODIS data are available twice a day because *Terra* and *Aqua* are polar-orbiting satellites. Therefore, the comparison was carried out at the times when MODIS data were available. Because of the continuous nature of GPS TPW data, the time difference between GPS and MODIS data was very small. The maximum distance separation allowed for data comparison between MODIS pixels and GPS TPW site locations was 10 km. For radiosondes, the maximum time and space differences between the launch site and the MODIS data pixels were 1.5 h and 30 km, respectively.

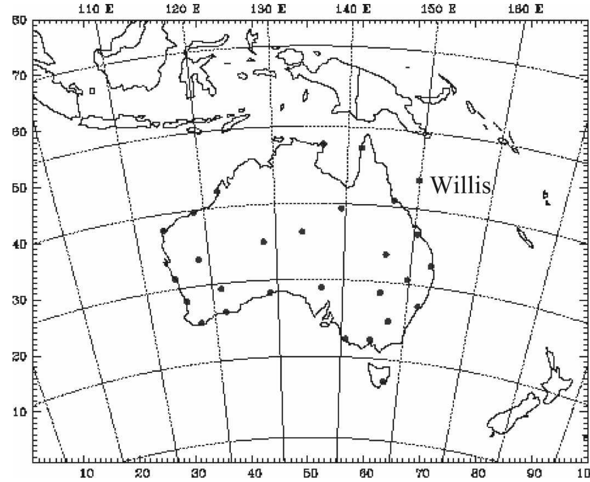

FIG. 2. The distribution of radiosonde stations over Australia.

b. Data comparison

About 2000 MODIS nIR and 6000 IR data points were compared with GPS TPW over the continental United States. In all of the nIR comparisons in this study, we excluded any points whose values were significantly underestimated (i.e., by more than 5 mm) as probably being due to the existence of clouds that were not accurately characterized by the cloud mask algorithm (i.e., those in the dashed box in Fig. 3a). Ideally, those underestimated points should be removed through the quality control process when they are assimilated. For nIR data, the retrieved TPW matched GPS TPW very well, particularly when MODIS TPW values were small (i.e., a drier atmosphere, Fig. 3). The MODIS nIR TPW was on average 1.8 mm moister than GPS TPW, as shown in Table 1, and the RMS of the differences between these two datasets was about 3.3 mm. The variation of the differences became larger as the column moisture content increased (Fig. 3a). MODIS IR TPW also matched GPS TPW quite well (Fig. 3b). The mean of the differences was about 0 mm and the RMS was 5.2 mm (Table 1). The variation was greater than that from nIR retrievals, implying that the uncertainty associated with MODIS IR TPW is greater than that with MODIS nIR TPW, and the range was almost independent of the column moisture amount.

Figure 4 shows the differences between MODIS TPW and GPS/radiosonde TPW and their linear regression relationships. Compared with GPS TPW (light gray crosses and light gray solid line in Fig. 4a), the MODIS nIR values were slightly underestimated in a dry atmosphere and overestimated in a moist atmosphere. The overestimation increased as the column water vapor content increased. A previous study com-

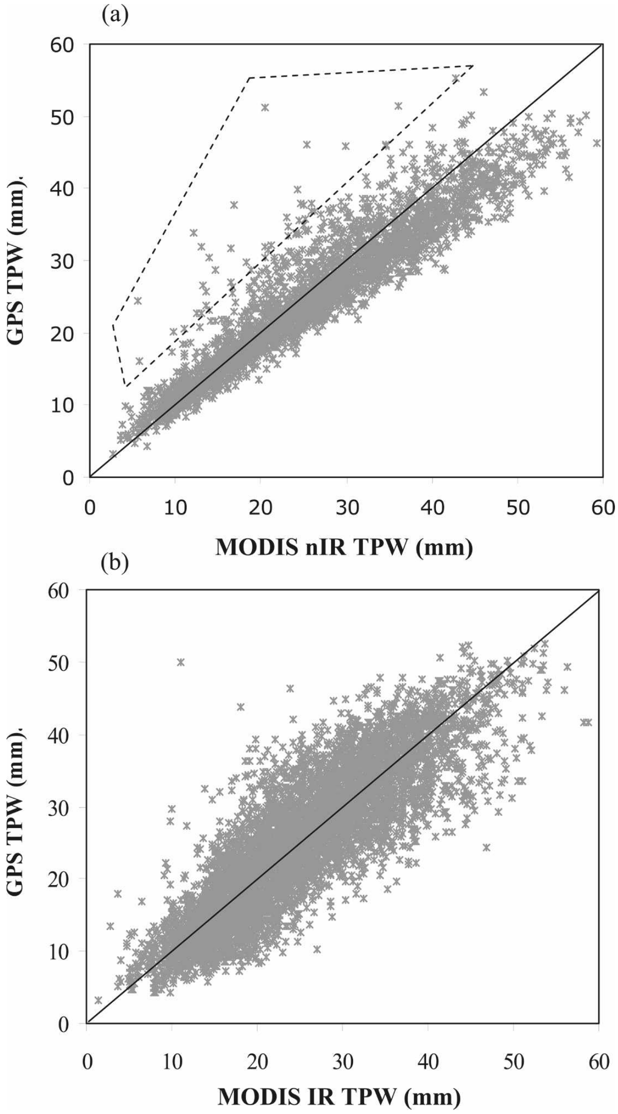

FIG. 3. Scatterplot for (a) MODIS nIR TPW vs GPS TPW and (b) MODIS IR TPW vs GPS TPW over the continental U.S. sites. Data were collected from 16 May to 9 Jun 2004. There were about 2000 and 6000 data points for nIR and IR, respectively. The dashed box in (a) highlights MODIS nIR points whose values were significantly underestimated.

paring MODIS data to a small number of data from only two sites (Li et al. 2003) also found an overestimation in a moist atmosphere. It showed MODIS TPW = 1.09 × GPS TPW − 0.3 mm for one site in England and MODIS TPW = 1.14 × GPS TPW − 0.1 mm for the ARM site in the U.S. Great Plains, whereas our study shows on average MODIS TPW = 1.14 × GPS TPW − 1.46 mm for 101 sites. The comparison here from a larger number of sites includes a much larger range of TPW values, up to 50 mm, and it is more robust for bias correction over a larger geographic region, especially at lower latitudes. Previous comparisons over sun-glint regions over ocean also found an underestimation of MODIS nIR TPW in a dry atmosphere, but there was no bias reported for a moist atmosphere (Kleidman et al. 2000).

Compared with GPS results, a similar regression trend (or slope) was shown in the difference between the MODIS nIR TPW and computed radiosonde TPW from the United States (116 data points; black-filled triangles and black solid line in Fig. 4a). However, the regression line has a higher positive bias. This was also shown in the comparison with radiosondes from Australia (about 550 data points; black opened circles and gray dashed line in Fig. 4a). This is consistent with the reported dry bias for moisture measurements from the RS80 and RS90 radiosondes (Wang et al. 2002; Miloshevich et al. 2006) that have been widely used in Australia and the United States, respectively. The mean differences in the radiosonde comparison, 3.5 and 2.8 mm for data from the United States and Australia, respectively, were larger than that in the GPS TPW comparison (Table 1). A comprehensive study comparing GPS and radiosonde data in Europe (Haase et al. 2003) showed that biases exist between the GPS and radiosonde data, with GPS data being moister overall. This bias, however, was shown to have an annual signal, and it was strongly associated with daytime radiosonde measurements, possibly indicating solar heating biases in the radiosondes. This is consistent with our results, which are also from daytime only.

For the MODIS IR data, comparison with GPS TPW (gray crosses and the gray line in Fig. 4b) indicated that the MODIS values were very likely overestimated for a dry atmosphere and underestimated for a moist atmosphere. The trend of the bias is consistent with that reported in Seemann et al. (2003). The comparison of MODIS IR TPW with radiosonde TPW over the United States and Australia also shows a similar result. The average differences of MODIS IR TPW from GPS TPW and from radiosondes over the United States were about 0 and 2.1 mm, respectively, and the difference from radiosondes over Australia were 1.5 mm (Table 1). This, again, shows that compared with GPS, lower values of moisture measurements were obtained from radiosonde instruments, in particular for a moist atmosphere (Fig. 4b). In this study, only GPS TPW data were used to estimate the bias of MODIS TPW because of the dry bias potentially associated with radiosonde data.

Figure 5 shows the differences of MODIS TPW from radiosonde TPW over Australia without removing any possibly suspect data. Results from Willis Island (refer to Fig. 2a for the location) were mostly underestimated

TABLE 1. The avg and the RMS for the differences of MODIS nIR and IR TPW from ground-based GPS TPW or radiosonde (RAD) TPW. Three datasets were used for comparison: 1) GPS data over U.S. sites from 16 May to 9 Jun 2004, 2) RAD data over Australia in 2003 January and July, and 3) RAD data over the United States 2002–05. MODIS data collected over the same period and region for each dataset were used. For MODIS nIR data, differences less than −5 mm were removed because of the possibility that the cloud mask was incorrect and data from Willis Island, Australia, were also removed. The No. of data points used in each comparison is also listed.

	MODIS nIR TPW			Corrected MODIS nIR TPW				MODIS IR TPW
	No.	Avg (mm)	RMS (mm)	Avg (mm)	RMS (mm)	No.	Avg (mm)	RMS (mm)
GPS (United States)	1998	1.8	3.3	0	2.0	6066	0	5.2
RAD (United States)	116	3.5	5.3	2.3	3.7	119	2.1	5.8
RAD (Australia)	505	2.8	4.0	2.3	3.2	807	1.5	5.7

for nIR data and mostly overestimated for IR data. This is quite different from other radiosonde sites in Australia. The observed MODIS TPW over this island might represent a marine atmosphere rather than a continental atmosphere. This systematic underestimation associated with the MODIS nIR TPW data on Willis Island could be due to lower reflectivity over the surrounding ocean region or due to the possibility that there was cloud around the island most of time. This implies that the bias of MODIS TPW data, either IR or nIR, over ocean can be very different from that over land. Because the GPS data that were used for bias estimation in this study were from the North American continent, the bias correction in the data assimilation study in section 3 was applied to data over land only.

c. *Bias correction for MODIS nIR TPW*

Based on the data comparisons, the uncertainty of the MODIS nIR TPW is smaller than the MODIS IR TPW. Therefore, in this study, only MODIS nIR data were corrected and evaluated using data assimilation and model simulations. Because of a dry bias associated with radiosonde data (Wang et al. 2002; Miloshevich et al. 2006), the bias of MODIS nIR TPW was estimated by comparing it with GPS TPW as shown in Fig. 4a (i.e., using GPS TPW as ground-truth observations). Data that had anomalously low MODIS nIR TPW values were excluded because they were potentially contaminated by cloudiness, and these data were likely to be screened out through the data quality control in data assimilation. The bias-corrected MODIS nIR TPW, TPW_n, in millimeters, was calculated as follows:

$$\mathrm{TPW}_n = (1 - 0.17) \times \mathrm{TPW}_o + 0.24, \qquad (1)$$

where TPW_o denotes the original MODIS nIR TPW value. This formula was used to correct MODIS nIR data in the numerical experiments in section 3. Note that (1) was derived from the correlation between the differences versus MODIS nIR TPW instead of the GPS TPW because the bias must be corrected based on the observed original MODIS TPW not the true TPW. The averaged differences of bias-corrected MODIS nIR TPW from GPS TPW over the United States and radiosondes over the United States and Australia were reduced to 0, 2.3, and 2.3 mm, respectively, and the RMS differences were improved to 2.0, 3.7, and 3.2 mm, respectively (Table 1).

3. Numerical configuration and experimental design

The Advanced Research WRF model (ARW), version 2 (Skamarock et al. 2005; Michalakes et al. 2001), was adopted for numerical simulations. The ARW model is a compressible three-dimensional (3D), nonhydrostatic model using terrain-following coordinates, and its governing equations are written in flux-form. The Runge–Kutta third-order time scheme was employed and the fifth- and third-order advection schemes were chosen for the horizontal and vertical directions, respectively. The WRF-VAR system (Skamarock et al. 2005) was successfully used to assimilate observations to improve model simulations and forecasts (Xiao and Sun 2007). In this study, the assimilation of MODIS TPW was developed and implemented in the WRF-VAR system to assess the impact of MODIS nIR TPW on severe weather simulations. The assimilation of SSM/I data was previously developed and tested (Chen et al. 2004), and the same methodology was applied here.

a. *Cases*

Two cases were studied: one over land and the other over ocean. The first case was a system of severe thunderstorms that occurred during early June 2004 over the central and southern United States. The storm system, producing strong wind and hail, moved southward from Oklahoma toward the northern border of Texas. Between 1710 UTC 2 June 2004 and 0120 UTC 3 June 2004, 61 reports of hail were registered with size rang-

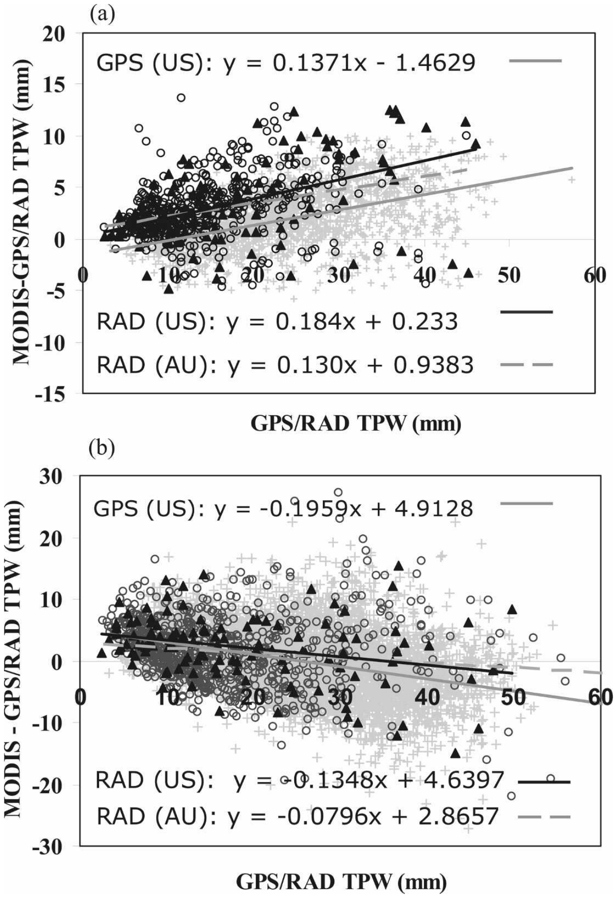

FIG. 4. Scatterplot for differences between MODIS TPW and RAD TPW (mm) vs RAD TPW (mm) over Australia (black opened circles) and over the United States (US; black filled triangles) and difference between MODIS TPW and GPS TPW (mm) vs GPS TPW (mm) over the United States (gray crosses) for (a) MODIS nIR and (b) MODIS IR data. For MODIS nIR data, the differences less than −5 mm were removed because of the possibility of an incorrect cloud mask and data from Willis Island, Australia (see Fig. 2 for location) were also removed. The linear regression lines are also plotted. For the comparison with radiosondes over the United States, there were 116 and 119 data points for MODIS nIR and IR, respectively. For the comparison with radiosondes over Australia, there were about 500 and 800 data points for nIR and IR, respectively.

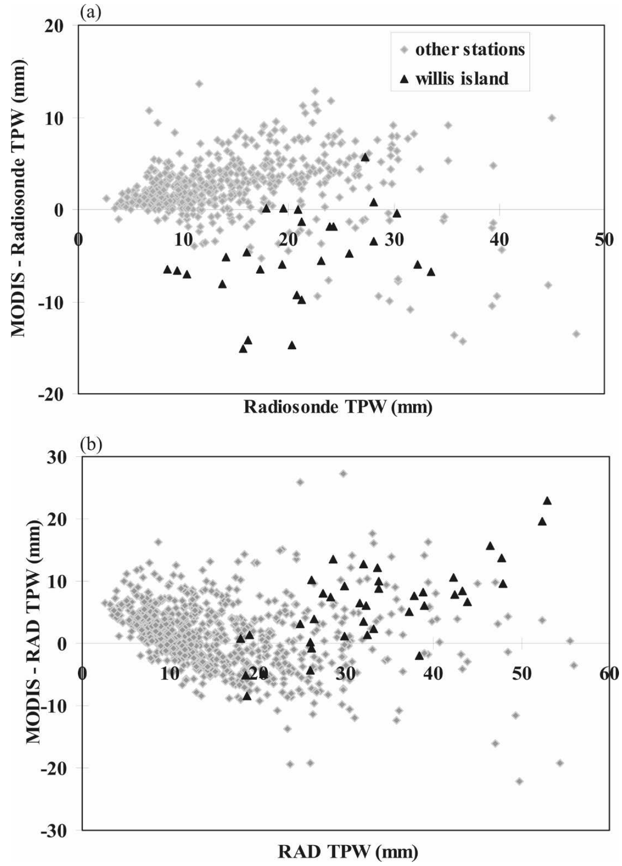

FIG. 5. (a) Scatterplot for the difference between MODIS nIR TPW and radiosonde TPW (mm) vs radiosonde TPW (mm) over Australia. (b) Same as (a) but for MODIS IR TPW. Black triangles indicate data from Willis Island, whereas the gray diamonds indicate data from other stations. Data used were collected from January and July 2003.

ing from 0.75 in. to 1.75 in. Later in the day on 2 June in Arkansas, hail-producing storms were spotted across the northern counties. In southwestern Arkansas, a line of strong-to-severe thunderstorms swept across the southern and western counties. The second case is Hurricane Isidore, which occurred in September 2002. Isidore started as a tropical wave off the coast of Africa on 9 September 2002, then it became a tropical storm around 0600 UTC 18 September. The storm was classified as a hurricane at 1800 UTC 19 September. Isidore reached a maximum intensity with winds of 55 m s^{-1} at 1800 UTC 21 September and a minimum sea level pressure (SLP) of 934 mb at 1200 UTC 22 September near the northern coast of the Yucatan. (More information about Isidore can be found in the National Hurricane Center tropical cyclone report online at www.nhc.noaa.gov/2002isidore.shtml.)

b. Numerical experiment design

Three sets of numerical experiments were conducted: one for the thunderstorms over land and the other two for Isidore over ocean. For each set, seven numerical experiments were designed, as shown in Table 2. Surface observations and radiosondes [global telecommunication system (GTS)], (original) MODIS nIR TPW from *Aqua* and *Terra*, bias-corrected MODIS nIR TPW, and retrieved SSM/I sea surface wind speeds and TPW were used for assimilation. The retrieved SSM/I data were available over ocean only. (MODIS data will

TABLE 2. Numerical experiments design. For the names and experiments, the first letter, L or O, denotes the case over land (i.e., severe thunderstorms over central-to-southern United States in 2004) or over ocean (i.e., Hurricane Isidore in 2002), respectively. The numbers 1 and 2 indicate the different sets of experiments for the Isidore case. The letters G, M, and B denote the conventional observations, (original) MODIS nIR TPW, and bias-corrected MODIS nIR TPW, respectively. Here, N indicates the control case in which no data were assimilated. For each experiment, the model was integrated 72 h, starting from 1800 UTC 1 Jun 2004, 1800 UTC 17 Sep 2002, and 1800 UTC 18 Sep 2002 for L, O1, and O2, respectively.

Expt			
Land/Great Plains	Ocean/Isidore 1	Ocean/Isidore 2	
1800 UTC 1 Jun 2004	1800 UTC 17 Sep 2002	1800 UTC 18 Sep 2002	Assimilated data
LN	O1N	O2N	None
LM	O1M	O2M	MODIS nIR TPW
LG	O1G	O2G	GTS (e.g., surface stations and radiosondes)
LGM	O1GM	O2GM	GTS + MODIS nIR TPW
LGB	O1GB	O2GB	GTS + Bias-corrected MODIS nIR TPW
LGS	O1GS	O2GS	GTS + SSM/I
LGSM	O1GSM	O2GSM	GTS + SSM/I + MODIS nIR TPW

refer to MODIS nIR data hereafter, unless otherwise specified.) Bias correction was performed on MODIS data pixels over land only in both the thunderstorm and hurricane cases.

A two-domain nested grid with two-way interactions with resolutions of 30 and 10 km was configured for all simulations. The grid dimensions were $144 \times 132 \times 31$ grid points for domain 1 and $226 \times 187 \times 31$ grid points for domain 2 in the east–west, north–south, and vertical directions, respectively. The following parameterizations were activated for both domains: Purdue–Lin microphysics scheme (Chen and Sun 2002), which is based on Lin et al. (1983) and Rutledge and Hobbs (1984) with some modifications; new Kain–Fritsch cumulus parameterization (Kain 2004), which includes deep and shallow convection; Yonsei University (YSU) boundary layer parameterization, which accounts for local and nonlocal mixing (Hong et al. 2006); Dudia shortwave parameterization (Dudia 1989); and Rapid Radiative Transfer Model (RRTM) long-wave parameterization (Mlawer et al. 1997). Reanalysis data from the Global Forecast System (GFS) with a spatial resolution of $1° \times 1°$ were used for boundary conditions and initial conditions. The model was integrated for 72 h with a time step of 90 s for domain 1 and 30 s for domain 2.

For each numerical experiment, a 6-h data cycling period with the assimilation of different observations was performed for both domains before the 72-h model integration (Tables 2 and 3). The assimilation of observations was carried out at exact hours with a 1-h time window centered at the analysis time of the 3DVAR (i.e., analysis time ± 0.5 h). Because some observations were assimilated into the GFS reanalysis, the assimilation of observations started 1 h after model integration during the 6-h data cycling period if observations were available. In this study, because the focus is MODIS data, to simplify the data cycling process the conventional observations (i.e., GTS) were assimilated only at those times when MODIS data were also available. As GTS data were used at three different times for the conducted experiments, their influence should be seen if there is any. Note that all second-set Hurricane Isidore assimilation (O2) experiments began with GFS reanalysis at 1200 UTC 18 September 2002 (i.e., cold start). For consistency, a 6-h data cycling period was also executed for LN, O1N, and O2N experiments prior to the 72-h integration, but no data were assimilated. Because there are no MODIS data available over the severe weather region (e.g., hurricane and convective clouds), the cold start model configuration (i.e., no clouds in the background field) will require some time for data outside this region to propagate in and potentially influence the severe weather simulation/forecast. In other words, the impact of MODIS data on severe weather simulations/forecasts might be delayed when using a cold start configuration.

c. *Error variances, data quality control, and data reduction for data assimilation*

To be conservative, the observational error input for MODIS TPW data was similar to, but slightly larger than, that estimated from the comparison with GPS data in section 2 (i.e., 3.3 and 2.0 mm for original and bias-corrected MODIS TPW, respectively). For the original MODIS data, an error of 4 mm was used for data over both land and ocean. After bias correction, which was applied to data over land only, an error of 2.5 mm was used over land and the value of 4 mm was maintained over ocean. Following Chen et al. (2004), the errors for retrieved SSM/I TPW and sea surface wind speeds were 2 mm and 2.5 m s^{-1}, respectively. For

TABLE 3. Observations that were assimilated during the data cycling period for each experiment listed in Table 2 for (a) the thunderstorm case over the central-to-southern United States, (b) the O1 experiments, and (c) the O2 experiments. The letters, G, M, B, and S, denote conventional data (GTS), including RAD and surface stations, original MODIS nIR TPW, bias-corrected MODIS nIR TPW, and SSM/I-retrieved sea surface wind speeds and TPW. The data cycling periods for L, O1, and O2 were 1200–1800 UTC 1 Jun 2004, 1200–1800 UTC 17 Sep 2002, and 1200–1800 UTC 18 Sep 2002, respectively. Here, 0–6 h corresponded to 1200–1800 UTC for each experiment during the data cycling period.

(a)

	0 h	1 h	2 h	3 h	4 h	5 h	6 h
LN							
LM						M	M
LG						G	G
LGM						GM	GM
LGB						GB	GB
LGS		S		S		G	G
LGSM		S		S		GM	GM

(b)

	0 h	1 h	2 h	3 h	4 h	5 h	6 h
O1N							
O1M					M	M	M
O1G					G	G	G
O1GM					GM	GM	GM
O1GB					GB	GB	GB
O1GS			S	S	G	G	G
O1GSM			S	S	GM	GM	GM

(c)

	0 h	1 h	2 h	3 h	4 h	5 h	6 h
O2N							
O2M				M		M	M
O2G				G		G	G
O2GM				GM		GM	GM
O2GB				GB		GB	GB
O2GS			S	GS	S	G	G
O2GSM			S	GSM	S	GM	GM

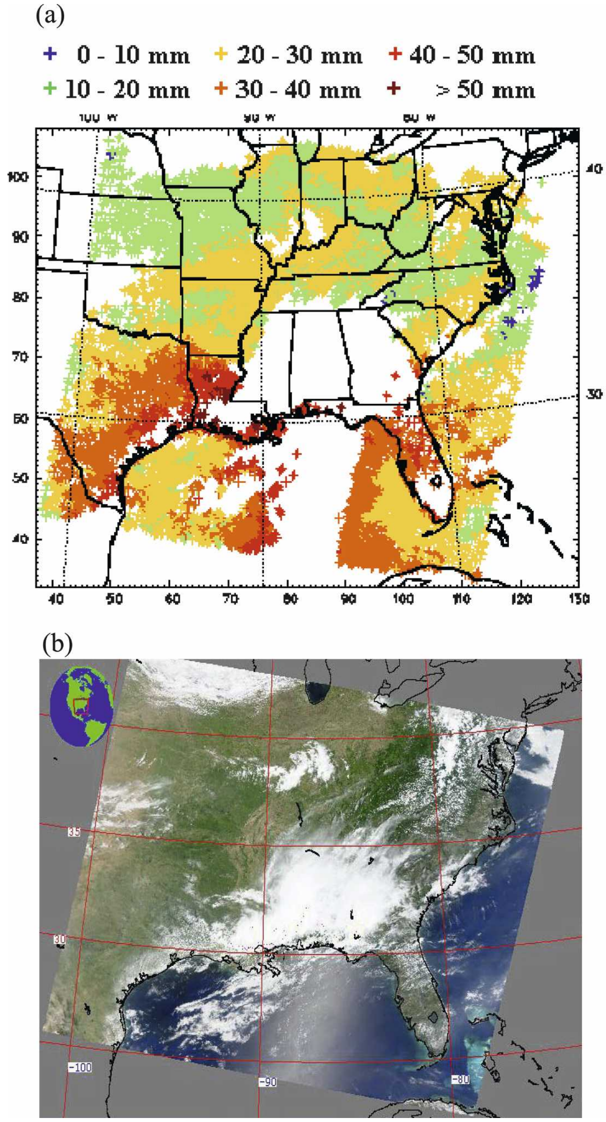

FIG. 6. (a) The coverage of retrieved MODIS nIR TPW after the screening of cloudy pixels. Data were collected from 1640 to 1645 UTC 1 Jun 2004. (b) MODIS satellite image from visible channels for the same period.

conventional observations, the default errors that came with the WRF-VAR package were used.

Three steps of data selection criteria were performed before MODIS TPW was assimilated. First, a 1-h time window centered at the analysis time (i.e., data assimilation time) was used to cut off data. This was applied to SSM/I data as well. Second, cloudy data were screened using the cloud flag in the MODIS dataset. As mentioned earlier, the nIR data were smoothed to a 5-km resolution from cloud-free pixels in 5×5 matrices, and a minimum of 10 clear-sky pixels was required. Figure 6a shows an example of the coverage of a 5-min MODIS TPW granule from 1640 to 1645 UTC 1 June 2004 after the removal of cloudy data. The results corresponded well to cloudy pixels identified by visual inspection of visible channels (Fig. 6b). Data over cloudy regions, such as southern Louisiana, Mississippi, Alabama, Georgia, and central northern Gulf of Mexico in Fig. 6, were removed. The last step was the gross error check. MODIS TPW data that differed from the model's background by more than 10 mm were excluded, whereas conventional and SSM/I data with differences greater than 5 times the observational standard deviation error, a default value, were removed. Because the prescribed observational errors were different for original and bias-corrected MODIS TPW (4 and 2.5 mm, respectively), a number of 10 mm instead of 5 times the observational standard deviation error was used for the

MODIS gross error check to keep the numbers of MODIS TPW data comparable in different experiments.

A simple data reduction process was performed on SSM/I and MODIS data to decrease the correlation of observations within the same grid box. If the data resolution was greater than the model horizontal resolution for each type of satellite observation, data were thinned by simply taking the average of the valid points within each grid box. Therefore, for each satellite data, at most one observation existed inside each grid box after the data reduction.

4. Numerical simulation results and discussion

a. Thunderstorm simulations in the central-to-southern United States

Figure 7 shows the SLP, 100-m wind speeds, and wind vectors of the thunderstorm case from the GFS reanalysis and 30-h model simulations at 0000 UTC 3 June 2004, within the period when high winds and heavy rainfall were observed over the Oklahoma region. In the GFS reanalysis (Fig. 7a), strong low-level northeasterly winds around central Oklahoma and southerly winds from western to central Texas with a maximum of about 10 $m s^{-1}$ formed a convergence zone over the border of these two states. The simulated winds in central Oklahoma from LN, which did not assimilate any data, and from LG, which assimilated conventional GTS data, were too weak and the location of maximum wind speeds was shifted to the southwest. Those with the assimilation of MODIS TPW, either with (LGB) or without (LGM, LM, and LGSM) bias correction, were stronger but the shift of the maximum wind location still existed. Through a nonlinear interaction, the assimilation of MODIS TPW could modify wind and temperature during model integration. Unfortunately, the simulated winds in southern Kansas and in the zone from northeast Mississippi to the border of Arkansas and Louisiana were too strong after assimilating MODIS data. The easterly component of simulated wind directions around central Oklahoma was too high for all experiments.

For the southerly wind from western to central Texas, simulated results from LN and LG did not pick up the right strength and direction because the low pressure system that propagated into domain 2 from the western boundary moved too slowly relative to the reanalysis. On the other hand, the simulated low pressure system from LM, LGM, and LGB propagated into domain 2 at approximately the right time as in the reanalysis, and the simulated strength and directions of southerly winds were more reasonable but slightly shifted northward. Therefore, the convergence zone over the border region between Oklahoma and Texas was better simulated in those tests with the assimilation of MODIS TPW (i.e., LM, LGM, and LGB) than the tests without (i.e., LN and LG). The simulated wind over the north to northeastern region of domain 2 was too strong (Fig. 7b) without the MODIS TPW, and it was slightly improved with MODIS TPW in northeastern Kansas and northern Missouri.

Results from the (additional) assimilation of SSM/I retrievals were unexpectedly similar to those from the assimilation of MODIS TPW (i.e., LGM versus LGMS and LGM versus LGS in Fig. 7), such as east-northeasterly winds in Oklahoma, southerly wind in Texas, and the low pressure system passing through the western boundary. This implies that the information from assimilating SSM/I data, which were available over ocean only, has been propagated inland and influenced the region of interest (i.e., Oklahoma and northern Texas). Compared with GFS reanalysis and LN, the assimilation of MODIS TPW was incapable of weakening low-level winds over northern Florida. This was improved slightly with GTS (Fig. 7c) and/or SSM/I data (Fig. 7g).

Figure 8 shows the observed and simulated 12-h accumulated rainfall from 1500 UTC 2 June to 0300 UTC 3 June 2004 (21–33-h simulation). Heavy precipitation was observed over eastern Oklahoma, the border region between Oklahoma and Texas, eastern Florida, and the area of Alabama, Georgia, and Florida near Tallahassee (Fig. 8a). The LN experiment did not reproduce rainfall over Oklahoma and eastern Florida (Fig. 8b). In addition, too much rainfall was generated in northern Louisiana. Simulated rainfall after the use of conventional GTS data (i.e., LG; Fig. 8c) was similar to that from LN but was slightly improved near Tallahassee. A false alarm was produced in southern Mississippi. Compared with LN, the assimilation of MODIS TPW in LM slightly improved the rainfall over the Oklahoma region because of an improved reproduction of the convergence zone mentioned earlier, but the amount and geographical extent were greatly underestimated; rainfall near Tallahassee (Fig. 8d) was slightly improved and the rainfall over northern Louisiana was removed. Neither LM nor LN reproduced rainfall in eastern Florida. The assimilation of GTS data plus MODIS TPW, either with or without bias correction, generated similar results to LM. However, the simulated precipitation near Tallahassee was shifted toward the northeast near the coast of Georgia. Rainfall over the Oklahoma region was also improved after assimilating SSM/I data (LGS and LGMS), in particular for the experiment that assimilated all observations

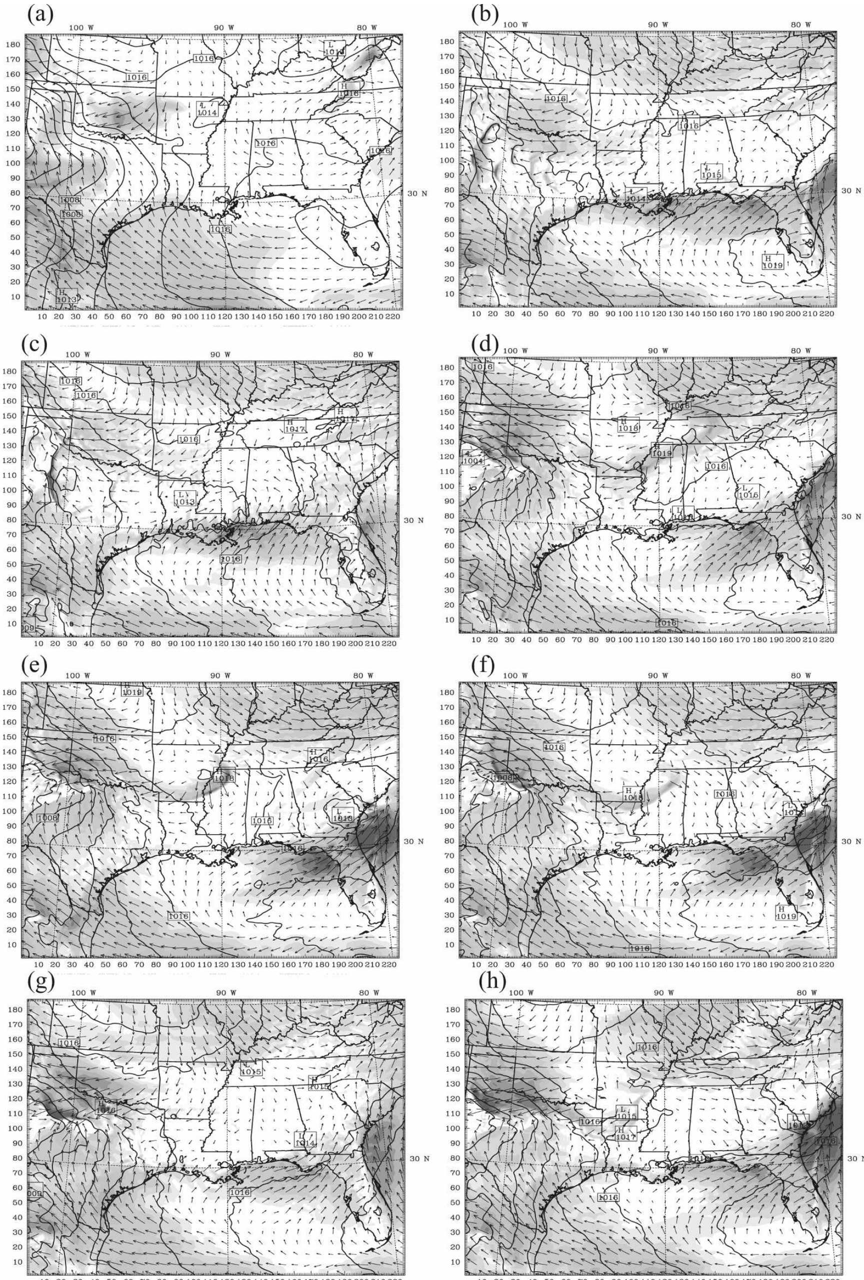

FIG. 7. SLP (contours) and wind speed (shaded) and vectors at 100-m height from (a) reanalysis and numerical expts of (b) LN, (c) LG, (d) LM, (e) LGM, (f) LGB, (g) LGS, and (h) LGMS for thunderstorm simulations at 0000 UTC 3 Jun 2004 after a 30-h simulation.

(LGMS). The simulated rainfall near Tallahassee was produced with LGS, though underestimated. Similar to LGM and LGB, the rainfall from LGMS was shifted toward the northeast.

Using 3-hourly outputs from the LM experiment, a backward trajectory for 10 points from the 27-h integration back to the initial time (i.e., from 2100 UTC 2 June back to 1800 UTC 1 June; Fig. 9) was calculated to determine the origin of the moisture contributing to those rainfall regions. Compared to LN, in addition to the improvement of the convergence zone over the border of Oklahoma and Texas (Fig. 7d), the precipitation over the Oklahoma region was improved because a source air mass that was traced back to eastern and southeastern Texas was moistened after the assimilation of MODIS TPW (LM), as shown in Fig. 10a. Fur-

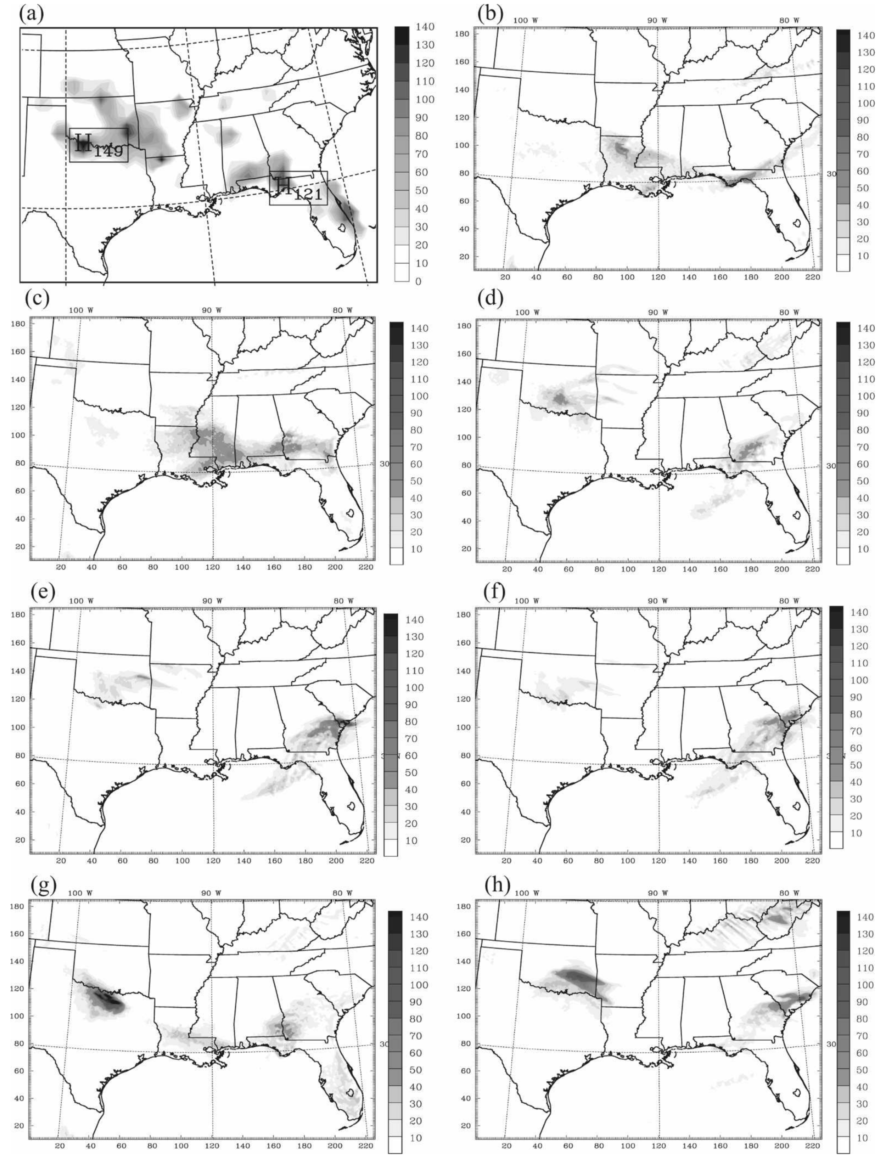

FIG. 8. (a) Observed and simulated 12-h accumulated rainfall from 1500 UTC 2 Jun to 0300 UTC 3 Jun 2004 for (b) LN, (c) LG, (d) LM, (e) LGM, (f) LGB, (g) LGS, and (h) LGMS for the thunderstorm simulations.

thermore, the removal of the false alarm in northern Louisiana and southern Mississippi (i.e., LN in Fig. 8b) was partially due to a reduction in moisture at the origins of the backward trajectories in southern Mississippi and western Alabama (Figs. 9 and 10a). Results from the thunderstorm simulations over the central and southern United States indicate that the simulated winds and rainfall for this case study can be slightly improved after the assimilation of MODIS data.

Figure 10b shows the difference of TPW between LGS and LG (LGS − LG). Note that SSM/I data, which were available over ocean only, were assimilated at an earlier time in the data cycling period (Table 3) and, therefore, had a chance to propagate over land. The increments after the assimilation of MODIS TPW and the assimilation of SSM/I retrievals in Fig. 10 present some similarities over land. However, the difference over ocean became more pronounced for this case. We suspect that retrieved SSM/I data, whose information was propagated over land during the data cycling period, had better quality, whereas MODIS nIR TPW data possibly had poorer quality over ocean and underestimated TPW. More studies on the improvement of MODIS nIR TPW and the error characteristics of these data over ocean through comparisons with other reliable observations are needed.

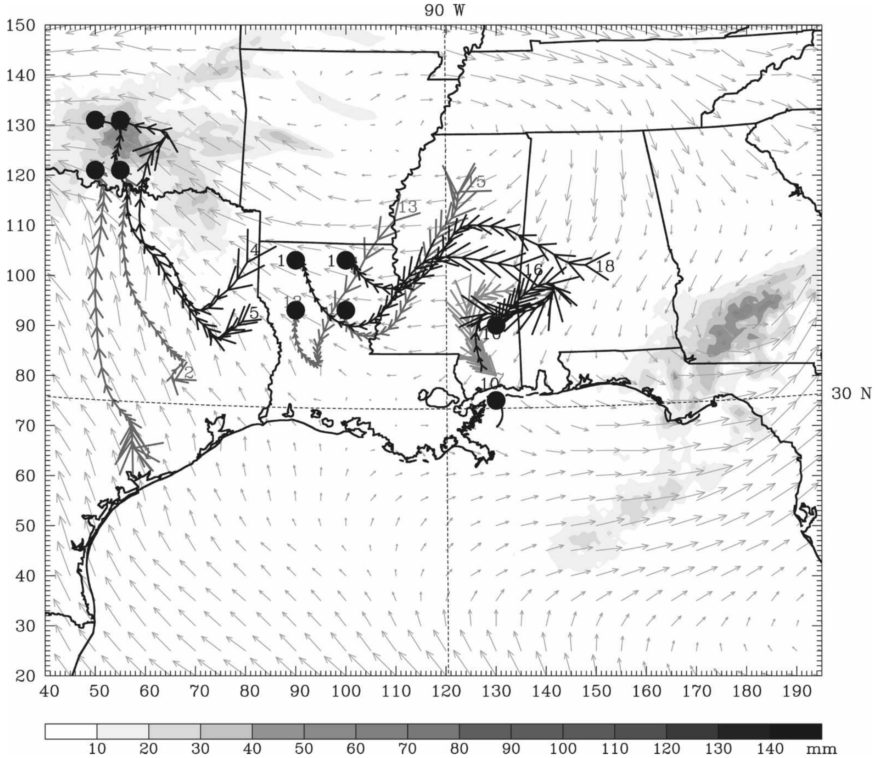

FIG. 9. Simulated backward trajectories from 27 (black points) to 0 h for the LM experiment. Simulated 12-h accumulated rainfall (shaded; mm) from 1500 UTC 2 Jun to 0300 UTC 3 Jun 2004 and wind vectors at 500-m height at 0300 UTC 3 Jun 2004 from the LM experiment are superimposed.

The difference between results after the use of MODIS TPW data with (i.e., LGM) and without (i.e., LGB) bias correction was not significant. The moisture increments for LGM and LGB (i.e., LGM − LN versus LGB − LN) at 1800 UTC 1 June 2004 were very similar, but LGM was slightly moister over high water vapor content regions (figure not shown). In this case study, although MODIS TPW data in the moist atmosphere were overestimated (i.e., larger innovation) in LGM, the use of a larger observational error (i.e., 4 mm) reduced the weight given to these data in data assimilation when compared to the assimilation with bias correction in LGB. The smaller weighting compensated for the effect of larger innovation values and it, therefore, suppressed the difference between LGM and LGB. Further systematic study of the influence of the bias correction on severe weather simulations/forecasts is required.

b. Hurricane Isidore simulations

1) O1 EXPERIMENTS

The first assimilation test carried out for Hurricane Isidore (O1) began with the 3DVAR analyses at 1800 UTC 17 September and ran to 1800 UTC 20 September 2002. Figure 11 shows three-day observed (i.e., from the best track positions) and simulated SLP at the storm's center and the maximum low-level wind speed. The observed storm slowly intensified over the first day as it skirted Jamaica. Then Isidore quickly increased its intensity, with a SLP of 967 hPa and maximum low-level wind of 45 m s^{-1} at 0600 UTC 20 September, before it approached Cuba, at which time the storm started weakening. At the end of the third day (1800 UTC 20 September), the SLP at the storm's center was 965 hPa and the maximum low-level wind was 37.5 m s^{-1}. Compared with observations, all simulated storm intensities were too weak for low-level wind from O1GS, except at the very end of the simulation. For O1N, which did not assimilate any observations during the cycling period, the SLP was 36-hPa higher and the maximum low-level wind was 23 m s^{-1} weaker than observed after a 72-h integration. The assimilation of any set of observations was able to increase the simulated storm intensity, except when only MODIS data were assimilated (i.e., O1M in Fig. 11).

It is interesting to see that the discrepancy in moisture between O1M and O1GM after the data cycling

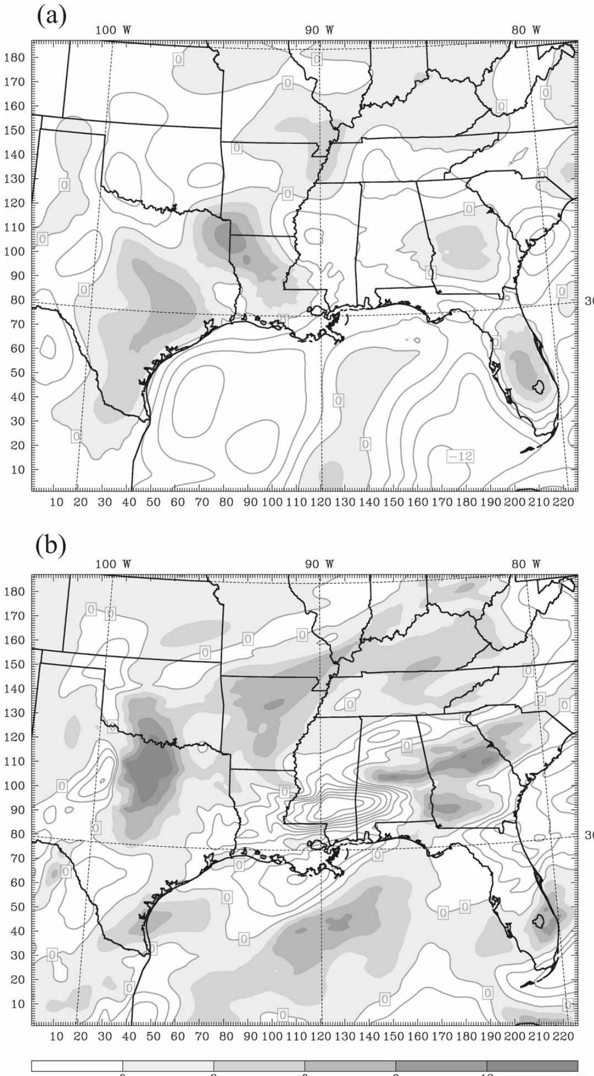

FIG. 10. Difference of TPW between (a) LM and LN and (b) LGS and LG at 1800 UTC 1 Jun 2004 after the 6-h data cycling. Shaded gray scales are positive values and contour lines are negative values.

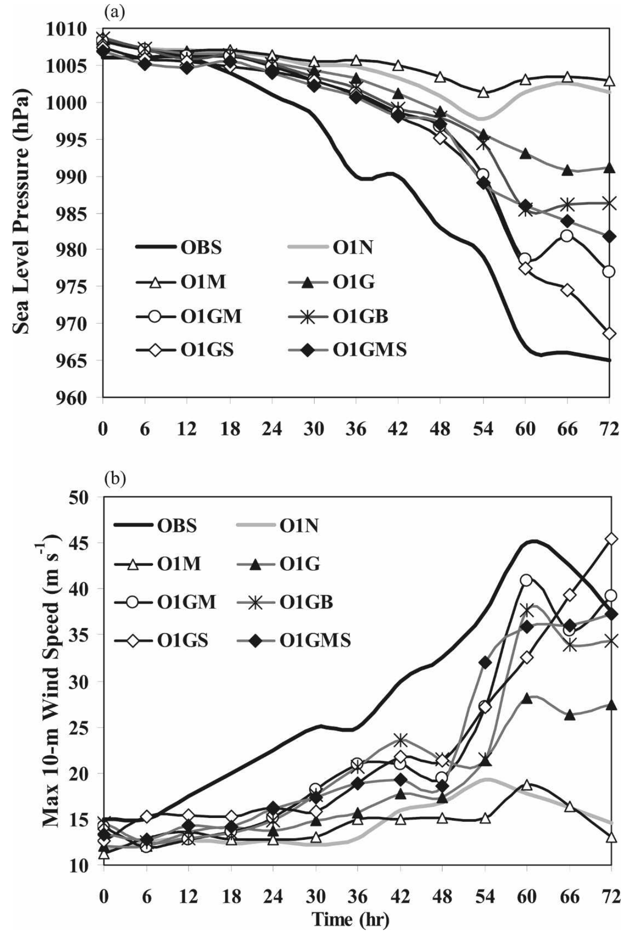

FIG. 11. Observed and simulated (a) SLP at the storm's center and (b) max 10-m wind speed from the O1 set of experiments. Time begins at 1800 UTC 17 Sep 2002.

(i.e., 1800 UTC 17 September 2000) was very minor (Fig. 12a versus Fig. 12b), but the simulated storm intensity from O1GM was much better than that from O1M (Fig. 11). For O1M, in addition to a slightly weaker simulated storm during the early integration period, the simulated track prevented the storm's development. The simulated storm deflected to the northeast of the observed track later in the simulation period and passed over Cuba. This inhibited the intensification of the storm because of the increase in surface friction and the decrease in the latent heat flux from the surface. This also occurred for the simulated track for O1N (Fig. 13a). The (additional) use of GTS data (e.g., O1GM) produced a northerly wind increment in the central region of domain 2 (i.e., Fig. 12a versus Fig. 12b in 500-hPa wind increments) and, in consequence, it partially corrected the simulated storm track to a much better direction (line G in Fig. 13b), allowing the storm to develop more strongly. The error was significantly reduced during the last one-and-half days (gray line with black-filled triangles in Fig. 14a), but the simulated storm still moved too slowly. Compared with O1N, the SLP at the storm's center deepened by 10 hPa, and the maximum low-level wind strengthened by 13 m s^{-1} after a 72-h integration (Fig. 11). With the addition of assimilating original MODIS data (i.e., O1GM), the simulated storm intensity was greatly enhanced after the correction of the simulated track. The enhancement was partially explained by the use of GTS data that effectively corrected the simulated storm direction with the northerly wind increments. However, the enhancement was also partially due to the use of MODIS data

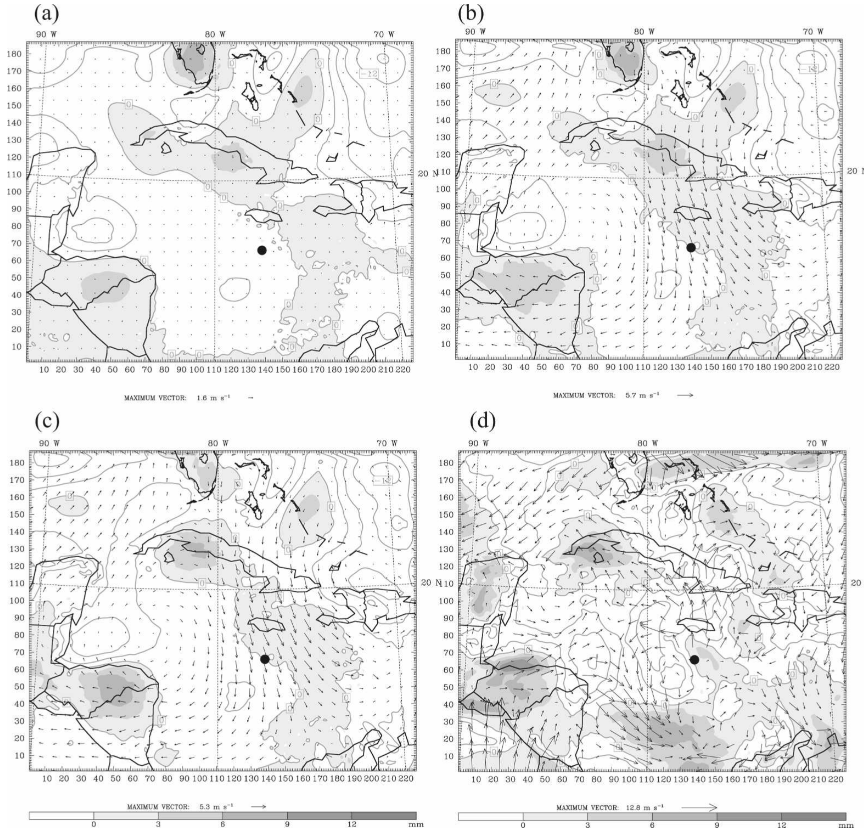

FIG. 12. TPW difference between (a) O1M and O1N, (b) O1GM and O1N, (c) O1GB and O1N, and (d) O1GS and O1G at 1800 UTC 17 Sep 2002 after the 6-h data cycling. Shaded gray scales are positive values and contour lines are negative values. Differences in wind vectors are plotted at 500 hPa for (a)–(c), and at 10-m for (d). The hurricane's location (black dot) is at 1800 UTC 17 Sep 2002. The region shown is domain 2.

because the improvement of the simulated intensity from O1GM was approximately double from that of O1G.

The pattern of the moisture increment from O1GB, which assimilated GTS data and bias-corrected MODIS TPW, was quite similar to that of O1GM, but the magnitudes were slightly different (Fig. 12c). The simulated storm intensities from O1GB and O1GM were close during the first two days (Fig. 11); the intensity from O1GB was slightly weaker during the third day. The use of SSM/I data produced a low-level divergence increment with a slightly cyclonic circulation around the simulated storm (Fig. 12d) and, unfortunately, increased the error of the initial storm position (Fig. 14a). The moisture increments due to the assimilation of MODIS TPW and the assimilation of SSM/I TPW were quite different over the ocean (Fig. 12a versus Fig. 12d). Nevertheless, the simulated storm intensity from O1GS was comparable to that of O1GM, except for the very last 12 h (Fig. 11). The simulated SLP at the storm's center deepened to 968.7 hPa, and the simulated maximum low-level wind reached 45.5 m s^{-1} at the end of the O1GS simulation. The direction of the simulated storm motion was reasonable, but the propagating speed was too slow. Simulated results after the additional use of MODIS TPW (i.e., O1GMS) were comparable to those from O1GS, but the simulated SLP and track were slightly worse for the last day. Although the error of the simulated track from O1GMS was relatively large compared with most of the other experiments (Figs. 13b and 14a), unlike O1N and O1M, the simulated storm was able to intensify because it stayed over the ocean during the simulation period. It is worth mentioning that a larger moisture increment around the storm area from O1GS implies that the influence of SSM/I data on the simulated storm could possibly be earlier than that of MODIS TPW because of a large data void area around the storm for MODIS TPW (i.e., cloudiness). Though this result is not clearly shown in the O1 experiments (Fig. 11), it becomes more evident in the O2 experiments, which are discussed in the next section.

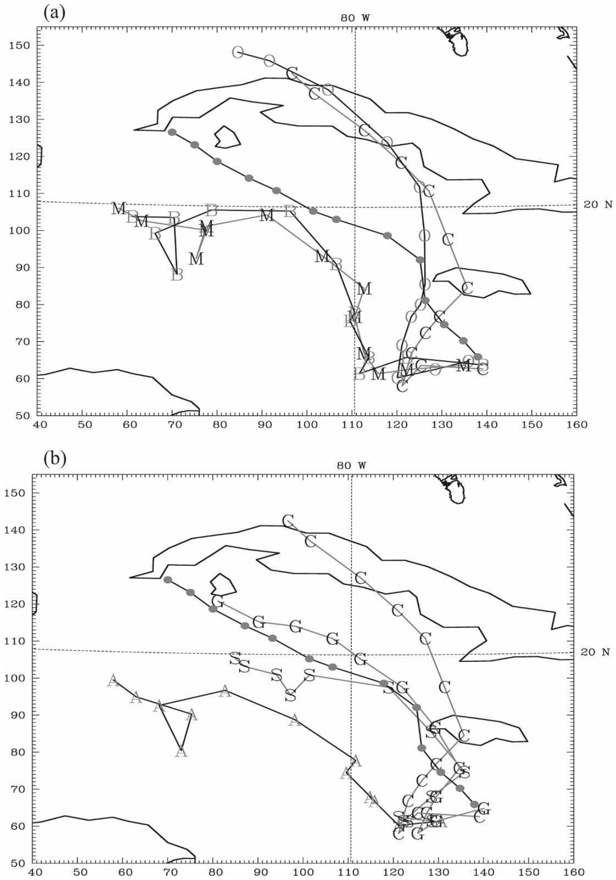

FIG. 13. Observed 72-h track (gray bullets) and simulated tracks from (a) O1N (black C), O1M (gray O), O1GM (black M), and O1GB (gray B), and (b) O1G (black G), O1GS (black S), and O1GMS (gray A) starting at 1800 UTC 17 Sep 2002. Observed and O1N are also plotted in (b) for comparison, with the same notation as in (a).

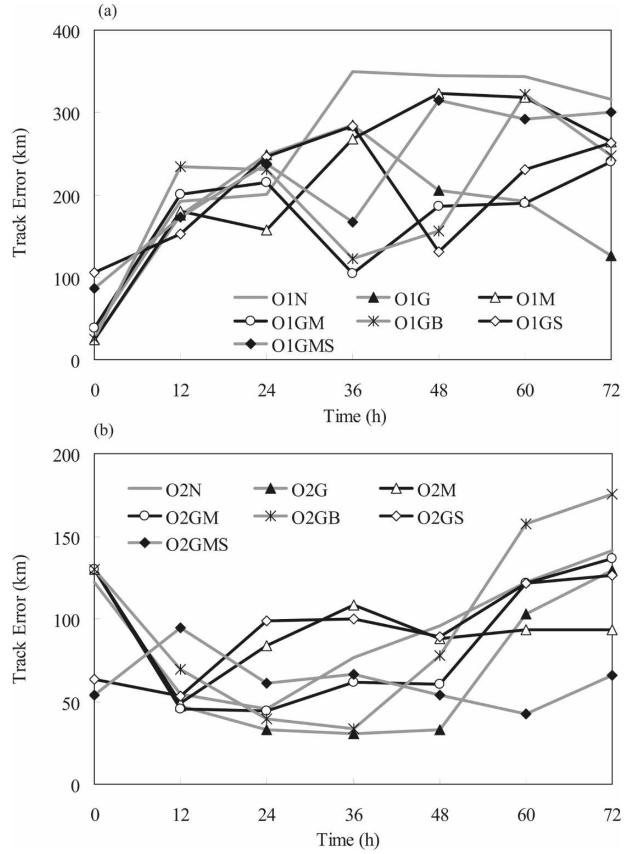

FIG. 14. Time evolution of simulated Isidore track error (km) for (a) O1 and (b) O2 experiments.

2) O2 EXPERIMENTS

The second set of assimilation tests carried out for Hurricane Isidore (O2) began with the 3DVAR analyses at 1800 UTC 18 September and ran to 1800 UTC 21 September 2002, which is shifted one day later than the O1 experiments. Some conclusions drawn from the data assimilation analysis from the O1 experiments were also reached with the O2 tests. A northerly wind anomaly over the central region of domain 2 was obtained after the use of GTS data (Fig. 15a). O2GM (Fig. 15a) and O2M produced similar moisture increments, as expected. The bias correction of MODIS TPW in O2GB, once again, did not make a significant difference in analysis compared to O2GM. As mentioned before, because of a larger data void area around the storm for MODIS TPW, the assimilation of SSM/I data provided a much more extensive area around the storm with a large moisture increment (Fig. 15a versus Fig. 15b). However, unlike O1GS, the assimilation of SSM/I data resulted in a saddle pattern of low-level wind increments (Fig. 15b), and the error of the initial storm position was reduced after the data cycling (Fig. 14b).

Figure 16 shows the observed and three-day simulated intensities for Isidore from the O2 experiments. Observed Isidore moved over the Caribbean Sea on the southwestern side of Cuba and intensified over 36 h. After that, the SLP stayed roughly constant, and the maximum low-level wind weakened when the storm approached, then it made landfall at the western edge of Cuba. Isidore regained strength after moving over the open ocean again. At 1800 UTC 21 September, that is, at 72 h, Isidore deepened to a SLP of 946 hPa and reached a maximum low-level wind of 55 m s^{-1}. In contrast to the O1 experiments, all simulated storm intensities were stronger than those observed after 30-h integrations and beyond, except that of O2GS from 36 to 42 h. At the end of the integrations, most of the simulated maximum low-level winds were close to the observed (Fig. 16b).

The simulated storm intensities from O2N and O2G

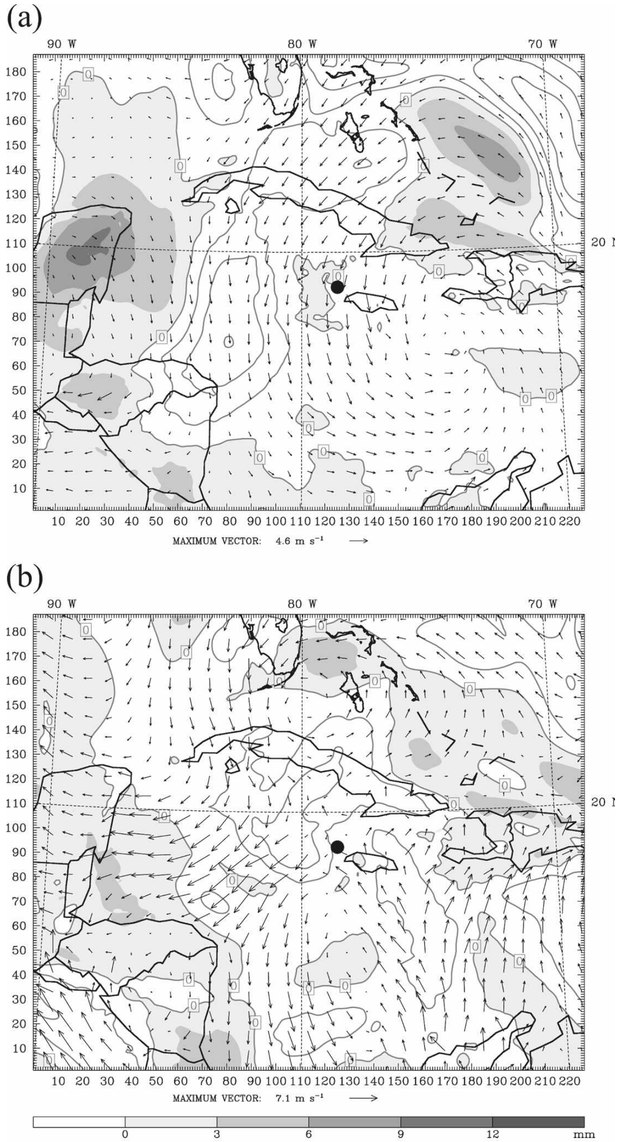

FIG. 15. TPW difference between (a) O2GM and O2N and (b) O2GS and O2G at 1800 UTC 18 Sep 2002 after the 6-h data cycling. Shaded gray scales are positive values and contour lines are negative values. Differences in wind vectors are plotted at 500 hPa for (a) and at 10 m for (b). The hurricane's (black dot) location is at 1800 UTC 18 Sep 2002.

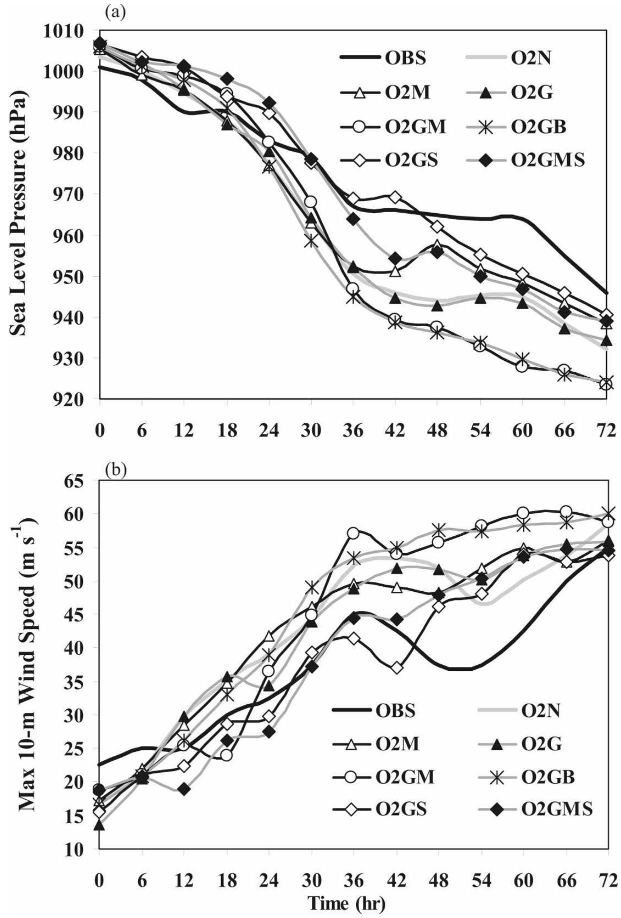

FIG. 16. Same as Fig. 11 but from the O2 set of experiments.

were very similar. Although both intensities were too strong, their trends were very close to the observed. Both simulated storm tracks passed over Isla de la Juventud, the small island to the south of western Cuba, then they turned left earlier than observed, skirting the southern coast of western Cuba (Fig. 17). The left turn had a similar weakening impact on the storm's intensity as the effect of crossing land on the observed storm track. The simulated storm from O2N moved northwestward with the track offset to the northeast relative to the observed. This shift was corrected when GTS data was assimilated (i.e., O2G) because of the northerly wind increment in the 3DVAR analysis (Fig. 15b). A similar conclusion was made regarding the simulated tracks in the O1 experiments. However, unlike O1G, the GTS data in O2G had no influence on the simulated storm intensity compared to O2N.

The results from O2M, O2GM, and O2GB show that MODIS TPW had almost no influence on the storm's intensity during the first one-and-a-half-day integration period. MODIS data started influencing the simulation of Isidore after 36 h. The assimilation of MODIS TPW (i.e., O2M) clearly improved the simulated intensity after 0600 UTC 20 September 2002 (i.e., after 36 h), and its trend was close to observed: the simulated storm made landfall in Cuba as observed. Compared with O2N, the simulated SLP from O2M was closer to the observed by 6.4 hPa at the end of the simulation.

The simulated storms from O2GM and O2GB were stronger than those from O2G and O2M, which were already stronger than the observed. The former two

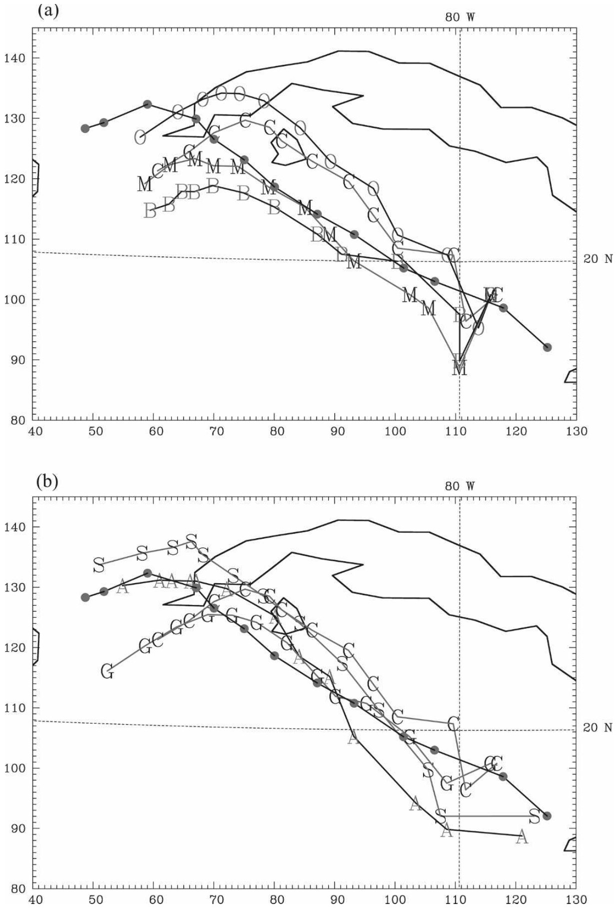

FIG. 17. Same as Fig. 13 but from the O2 set of experiments and starting at 1800 UTC 18 Sep 2000.

experiments displayed no weakening or steady-state period in the storms' intensities (Fig. 16). This is because the simulated track from O2GB was shifted too far to the west, and the simulated track from O2GM moved too slowly (e.g., it approached the Isla de la Juventud 6 h later than observed) and both turned left before the simulated storms were affected by passing over western Cuba (Fig. 17a). The discrepancies between the simulated storm intensities from O2GM and O2GB were indistinguishable (Fig. 16).

The assimilation of SSM/I data (e.g., O2GS), which were available over the cloudy areas over ocean, influenced the simulated storms after an 18-h integration, which was earlier than the effects from MODIS data (e.g., O2GM). This can be seen in the greater extent of the region with a large negative TPW increment around the storm, as mentioned earlier (Fig. 15a versus Fig. 15b). The primary reason for this was because MODIS data were void around the storm. The simulated storm from O2GS moved across western Cuba, similar to the observed track, though a little farther northeast, and its simulated intensity was better than those from the other O2 experiments (Fig. 16). The simulated SLP at the storm's center was only 940.5 hPa, which was 8.5 hPa better than the SLP from O2N. O2GMS also greatly improved the simulated storm intensity. The error in the simulated track was close to a constant over the whole simulation period, causing its track to outperform others on the third day (Fig. 17b). In general, the O2 experiments better simulated tracks (Fig. 13 versus Fig. 17), and they had significantly lower errors than the O1 experiments (Fig. 14a versus Fig. 14b), which started model integrations one day earlier.

5. Concluding remarks

Comparisons of MODIS TPW and GPS TPW over the continental United States showed that the RMS differences between GPS and the two MODIS data products were about 5.2 and 3.3 mm for IR and nIR TPW, respectively. This implies that nIR retrievals are more precise than the IR retrievals. Results also showed that MODIS IR TPW data were overestimated in a dry atmosphere but underestimated in a moist atmosphere. In contrast, the nIR values were slightly underestimated in a dry atmosphere but overestimated in a moist atmosphere. After applying a bias correction, the RMS difference between MODIS nIR TPW and GPS TPW was reduced to 2 mm over land. The trends in the differences between MODIS TPW and radiosonde TPW over the United States and Australia were similar to those from GPS TPW, but the differences were larger. This could be because of the potential dry bias associated with radiosonde measurements reported in previous studies (Wang et al. 2002; Miloshevich et al. 2006). The comparison results suggest that the bias of MODIS TPW over ocean (i.e., results from Willis Island) could be very different from that over land and merits further study. For this reason, the bias correction was applied only to MODIS nIR TPW over land when assimilating the data.

The assimilation of MODIS nIR TPW data, along with conventional GTS data and SSM/I retrievals, into WRF model simulations was demonstrated for a severe thunderstorm case over the central-to-southern United States in early June 2004 and for Hurricane Isidore over ocean in September 2002. For each experiment, a 6-h data cycling before model integration was performed with the assimilation of different observations. The results of the thunderstorm case over land show that the assimilation of MODIS nIR data slightly improved simulated rainfall over the region of interest in southern Oklahoma. This was because the low-level convergence in that area was better simulated and because the moisture at the source, which was traced back to southeastern Texas, increased after the use of MODIS nIR TPW data. Interestingly, the impact of SSM/I retrievals on simulated wind and rainfall for the thunderstorm case study was similar to that of MODIS nIR TPW. Although SSM/I data were available only over the ocean, their influence was propagated over land after those data were assimilated. The influence of conventional GTS data on this particular case study was negligible, possibly because the quality of the reanalysis data over land was relatively good compared to over the ocean; in addition, only limited data were used (i.e., GTS data were assimilated only at the times when MODIS data were available).

Simulated intensities from the Isidore O1 experiments, which started at 1800 UTC 17 September 2002, were all too weak, especially when there was a large error in the simulated tracks (i.e., O1N and O1M). However, MODIS nIR TPW with the additional use of conventional GTS data (i.e., O1GM) greatly improved the simulated storm intensity. The improvement was partially explained by the northerly wind increments produced when using the GTS data that effectively corrected the simulated storm direction. Moreover, the improvement was also partially due to MODIS data because the improvement of the simulated intensity from O1GM was approximately double from that of O1G. In contrast, the simulated intensities from the Isidore O2 experiments, which started at 1800 UTC 18 September 2002, were too strong for the last one-and-a-half days. The error of the simulated storm track from O2N was smaller than that from O1N. With a better simulated track, the use of MODIS nIR data alone (i.e., O2M) was able to improve the simulated storm intensity after a 36-h integration. Although GTS data still had a positive impact on the simulated track in O2G, it did not improve the simulated storm intensity. Unlike O1GM, the use of MODIS nIR TPW and GTS data (i.e., O2GM) worsened the simulation results (i.e., the storm was too strong) compared to O2N because the simulated storm moved too slowly and turned left too early when it approached western Cuba. Although simulated results from the O1 experiments were quite different from the O2 experiments, some conclusions were similar. In general, GTS data in some cases had a positive impact on the simulated track, in particular the storm's moving direction; the accuracy of the simulated storm intensity greatly depended on the simulated track (e.g., whether it reached landfall or not); the assimilation of MODIS nIR TPW improved the simulated intensity when the simulated track was reasonably well reproduced; and the simulated storm intensity with the use of SSM/I data was comparable to or slightly better than when using the MODIS nIR data. Note that the influence of MODIS data on the storm simulation can be delayed because no full column water vapor data over cloudy regions are available, whereas SSM/I data, which are available over cloudy areas, can influence the storm simulation earlier. This was clearly shown in the O2 experiments.

The difference in the moisture increments after assimilating MODIS nIR data with and without bias correction was relatively minor when compared with the differences between assimilating MODIS and the assimilation of other types of observations (i.e., SSM/I or GTS). This is perhaps because any overestimation of the MODIS nIR TPW data was compensated by the use of a larger observational error (i.e., less weighting) when compared with the use of bias-corrected data. Further systematic evaluation of the effect of the bias correction and investigation of the bias over ocean are needed. Nevertheless, this preliminary work demonstrates that MODIS data can have a positive impact relative to other types of data, and MODIS data have the potential to improve weather simulations and forecasts. More case studies are required to further substantiate these conclusions.

The cloud information from MODIS data can be useful to represent storms' structures. The assimilation of this type of data is very important but challenging. Although some skills have been developed to take into account cloud observations, such as 4DVAR, it is relatively more difficult to assimilate this type of data using 3DVAR because of the lack of good balance constraints regarding the cloud field. The research in this direction is still wide open and more efforts are indeed needed in the future.

Acknowledgments. The authors would like to acknowledge the WRF model and WRF-VAR development teams for their efforts on model development. We would also like to thank Jack Kain at NSSL/NOAA for his help on our severe storm case selection, Debbie Shutts and Eric Calais for their contributions to the GPS data processing, and Dennis Shea for his assistance with NCL. The MODIS data were obtained from the NASA Goddard Earth Sciences Data and Information Services Center. The GPS data were obtained from the NOAA Forecasts Systems Laboratory. The SSM/I data were obtained from the Global Hydrology Resource Center at the Global Hydrology and Climate Center, NASA, Huntsville, Alabama. This work is supported by NASA Grant NNG04GM90G 521 NRA 03-OES-02. Additional support is provided by the University of California Toxic Substances Research and Teaching Program (TSR&TP) through the Atmospheric Aerosols and Health Lead Campus Program.

REFERENCES

Andrew, M. C., 1987: Satellite-derived attributes of cloud vortex systems and their application to climate studies. *Remote Sens. Environ.,* **22,** 271–296.

Chelton, D. B., and F. J. Wentz, 2005: Global microwave satellite observations of sea surface temperature for numerical weather prediction and climate research. *Bull. Amer. Meteor. Soc.,* **86,** 1097–1115.

Chen, S.-H., 2007: The impact of assimilating SSM/I and QuikSCAT satellite winds on Hurricane Isidore simulations. *Mon. Wea. Rev.,* **135,** 549–566.

——, and W.-Y. Sun, 2002: A one-dimensional time-dependent cloud model. *J. Meteor. Soc. Japan,* **80,** 99–118.

——, F. Vandenberghe, G. W. Petty, and J. F. Bresch, 2004: Application of SSM/I satellite data to a hurricane simulation. *Quart. J. Roy. Meteor. Soc.,* **130,** 801–825.

Deblonde, G., 1999: Variational assimilation of SSM/I total precipitable water retrievals in the CMC analysis system. *Mon. Wea. Rev.,* **127,** 1458–1476.

Dudia, J., 1989: Numerical study of convection observed during the winter monsoon experiment using a mesoscale two-dimensional model. *J. Atmos. Sci.,* **46,** 3077–3107.

Gao, B.-C., and Y. J. Kaufman, 2003: Water vapor retrievals using Moderate Resolution Imaging Spectroradiometer (MODIS) near-infrared channels. *J. Geophys. Res.,* **108,** 4389, doi:10.1029/2002JD003023.

Gerard, E., and R. W. Saunders, 1999: Four-dimensional variational assimilation of Special Sensor Microwave/Imager total column water vapour in the ECMWF model. *Quart. J. Roy. Meteor. Soc.,* **125,** 3077–3101.

Gutman, S. I., S. R. Sahm, S. G. Benjamin, B. E. Schwartz, K. L. Holub, J. Q. Stewart, and T. L. Smith, 2004: Rapid retrieval and assimilation of ground based GPS precipitable water observations at the NOAA Forecast Systems Laboratory: Impact on weather forecasts. *J. Meteor. Soc. Japan,* **82,** 351–360.

Haase, J., M. Ge, H. Vedel, and E. Calais, 2003: Accuracy and variability of GPS tropospheric delay measurements of water vapor in the western Mediterranean. *J. Appl. Meteor.,* **42,** 1547–1568.

Hong, S.-Y., Y. Noh, and J. Dudhia, 2006: A new vertical diffusion package with an explicit treatment of entrainment processes. *Mon. Wea. Rev.,* **134,** 2318–2341.

Hou, A. Y., D. V. Ledvina, A. M. da Silva, S. Q. Zhang, J. Joiner, R. M. Atlas, G. J. Huffman, and C. D. Kummerow, 2000: Assimilation of SSM/I-derived surface rainfall and total precipitable water for improving the GEOS analysis for climate studies. *Mon. Wea. Rev.,* **128,** 509–537.

Huang, C.-Y., Y.-H. Kuo, S.-H. Chen, and F. Vandenberghe, 2005: Improvements in typhoon forecasts with assimilated GPS occultation refractivity. *Wea. Forecasting,* **20,** 931–953.

Huang, J., P. Minnis, B. Lin, T. Wang, Y. Yi, Y. Hu, S. Sun-Mack, and K. Ayers, 2006: Possible influences of Asian dust aerosols on cloud properties and radiative forcing observed from MODIS and CERES. *Geophys. Res. Lett.,* **33,** L06824, doi:10.1029/2005GL024724.

Isaksen, L., and P. A. E. M. Janssen, 2004: Impact of ERS scatterometer winds in ECMWF's assimilation system. *Quart. J. Roy. Meteor. Soc.,* **130,** 1793–1814.

Kain, J. S., 2004: The Kain–Fritsch convective parameterization: An update. *J. Appl. Meteor.,* **43,** 170–181.

Kaufman, Y. J., and B.-C. Gao, 1992: Remote sensing of water vapor in the near IR from EOS/MODIS. *IEEE Trans. Geosci. Remote Sens.,* **30,** 871–884.

King, M. D., Y. J. Kaufman, W. P. Menzel, and D. Tanre, 1992: Remote sensing of cloud, aerosol, and water vapor properties from the moderate resolution imaging spectrometer (MODIS). *IEEE Trans. Geosci. Remote Sens.,* **30,** 2–27.

——, and Coauthors, 2003: Cloud and aerosol properties, precipitable water, and profiles of temperature and water vapor from MODIS. *IEEE Trans. Geosci. Remote Sens.,* **41,** 442–458.

Kleidman, R. G., Y. J. Kaufman, B.-C. Gao, L. A. Remer, V. G. Brackett, R. A. Ferrare, E. V. Browell, and S. Ismail, 2000: Remote sensing of total precipitable water vapor in the near-IR over ocean glint. *Geophys. Res. Lett.,* **27,** 2657–2660.

Lagouvardos, K., and V. Kotroni, 2005: Improvement of high-resolution weather forecasts through humidity adjustment based on satellite data source. *Quart. J. Roy. Meteor. Soc.,* **131,** 2695–2712.

Lau, K.-M., and P. H. Chan, 1983: Short-term climate variability and atmospheric teleconnections from satellite-observed outgoing longwave radiation. Part II: Lagged correlation. *J. Atmos. Sci.,* **40,** 2751–2767.

Leidner, S. M., L. Isaksen, and R. N. Hoffman, 2003: Impact of NSCAT winds on tropical cyclones in the ECMWF 4DVAR assimilation system. *Mon. Wea. Rev.,* **131,** 3–26.

Li, Z. H., J.-P. Muller, and P. Cross, 2003: Comparison of precipitable water vapor derived from radiosonde, GPS, and Moderate-Resolution Imaging Spectroradiometer measurements. *J. Geophys. Res.,* **108,** 4651, doi:10.1029/2003JD003372.

Liljegren, J., B. Lesht, T. VanHove, and C. Rocken, 1999: A comparison of integrated water vapor from microwave radiometer, balloon-borne sounding system and Global Positioning System. *Extended Abstracts, Ninth Atmospheric Radiation Measurement Program Science Team Meeting,* San Antonio, TX, U.S. Department of Energy, 1–8.

Lin, Y.-L., R. D. Farley, and H. D. Orville, 1983: Bulk parameterization of the snow field in a cloud model. *J. Climate Appl. Meteor.,* **22,** 1065–1092.

Michalakes, J., S.-H. Chen, J. Dudhia, L. Hart, J. Klemp, J. Middlecoff, and W. Skamarock, 2001: Development of a next generation regional Weather Research and Forecast Model. *Developments in Teracomputing: Proceedings of the Ninth ECMWF Workshop on the Use of High Performance Computing in Meteorology,* W. Zwieflhofer and N. Kreitz, Eds., World Scientific, 269–276.

Miloshevich, L. M., H. Vömel, D. N. Whiteman, B. M. Lesht, F. J. Schmidlin, and F. Russo, 2006: Absolute accuracy of water vapor measurements from six operational radiosonde types launched during AWEX-G and implications for AIRS validation. *J. Geophys. Res.,* **111,** D09S10, doi:10.1029/2005JD006083.

Mlawer, E. J., S. J. Taubman, P. D. Brown, M. J. Iacono, and S. A. Clough, 1997: Radiative transfer for inhomogeneous atmospheres: RRTM, a validated correlated-k model for the longwave. *J. Geophys. Res.,* **102,** 16 663–16 682.

Pu, Z.-X., and S. A. Braun, 2001: Evaluation of bogus vortex techniques with four-dimensional variational data assimilation. *Mon. Wea. Rev.,* **129,** 2023–2039.

Rocken, C., R. Ware, T. Van Hove, F. Solheim, C. Alber, J. Johnson, M. Bevis, and S. Businger, 1993: Sensing atmospheric water vapor with the Global Positioning System. *Geophys. Res. Lett.,* **20,** 2631–2634.

Rutledge, S. A., and P. V. Hobbs, 1984: The mesoscale and microscale structure and organization of clouds and precipitation in midlatitude cyclones. XII: A diagnostic modeling study of precipitation development in narrow cloud-frontal rainbands. *J. Atmos. Sci.,* **41,** 2949–2972.

Seemann, S. W., J. Li, W. P. Menzel, and L. E. Gumley, 2003: Operational retrieval of atmospheric temperature, moisture, and ozone from MODIS infrared radiances. *J. Appl. Meteor.,* **42,** 1072–1091.

Skamarock, W., J. Klemp, J. Dudhia, D. Gill, D. Barker, W. Wang, and J. Powers, 2005: A description of the advanced research WRF version 2. NCAR Tech. Note NCAR/TN-468+STR, 100 pp.

Smith, T. L., S. G. Benjamin, B. E. Schwartz, and S. I. Gutman, 2000: Using GPS-IPW in a 4-D data assimilation system. *Earth Planets Space,* **52,** 921–926.

Steffen, K., W. Abdalati, and J. Stroeve, 1993: Climate sensitivity studies of the Greenland ice sheet using satellite AVHRR, SMMR, SSM/I and in situ data. *Meteor. Atmos. Phys.,* **51,** 239–258.

Wang, J., H. Cole, D. J. Carlson, E. R. Miller, K. Beierle, A. Paukkunen, and T. K. Laine, 2002: Corrections of humidity measurement errors from the Vaisala RS80 radiosonde—Application to TOGA COARE data. *J. Atmos. Oceanic Technol.,* **19,** 981–1002.

Wang, X., and D. V. Michelangeli, 2006: Comparison of microphysical modeling of polar stratospheric clouds against balloon-borne and Improved Limb Atmospheric Spectrometer (ILAS) satellite observations. *J. Geophys. Res.,* **111,** D10201, doi:10.1029/2005JD006222.

Xiao, Q., and J. Sun, 2007: Multiple-radar data assimilation and short-range quantitative precipitation forecasting of a squall line observed during IHOP_2002. *Mon. Wea. Rev.,* **135,** 3381–3404.

——, X. Zou, and Y.-H. Kuo, 2000: Incorporating the SSM/I-derived precipitable water and rainfall rate into a numerical model: A case study for the ERICA IOP-4 cyclone. *Mon. Wea. Rev.,* **128,** 87–108.

Zhang, X., Q. Xiao, and P. Fitzpatrick, 2007: The impact of multisatellite data on the initialization and simulation of Hurricane Lili's (2002) rapid weakening phase. *Mon. Wea. Rev.,* **135,** 526–548.

Zou, X., Q. Xiao, A. E. Lipton, and G. D. Modica, 2001: A numerical study of the effect of GOES sounder cloud-cleared brightness temperatures on the prediction of Hurricane Felix. *J. Appl. Meteor.,* **40,** 34–55.